BIOPOLYMER COATED MESOPOROUS SILICA NANOPARTICLES FOR CONTROLLED THERAPEUTIC DELIVERY: BATTLE FOR BIOAVAILABILITY

by

Michael C Harget

A thesis submitted to the Faculty and the Board of Trustees of the Colorado School of Mines in partial fulfillment of the requirements for the degree of Master of Science (Applied Chemistry).

Golden, Colorado

Date _____

Signed: _____

Michael C Harget

Signed: _____

Dr. Brian G Trewyn
Thesis Advisor

Golden, Colorado

Date _____

Signed: _____

Dr. Thomas Gennett
Professor and Department Head
Department of Chemistry

ABSTRACT

Traditional drug delivery methods are unable to alleviate challenges associated with the administration of medicine, which include non-target site exposure, adverse effects, environmental impact, and unnecessary cost.[1-3] In addition to continual drug development, it is equally or more important to consider new methods to use traditional drugs with higher efficiency.[4] Mesoporous silica nanoparticles provide an alluring avenue towards a stimulus specific biomolecule and drug delivery system due to their high surface area (over 1,000 m^2/g), biocompatibility, and chemical tailorability.[5-7] The well-defined pores of MSN materials can host and actively release drug molecules in a controlled manner, reducing non-target site exposure and adverse effects while improving patient compliance and overall treatment effectiveness.[8-10] To achieve this, various materials have been explored as endcaps to trap payloads within the pores of MSN until reaching a specific stimulus that releases the therapeutic.[11-12] The biological compatibility and relevance of the biopolymer amylose makes it a suburb candidate for pore coverage.[3,13] Amylose nanoparticles have been pursued in literature for topical drug delivery and wound dressing.[14-16] Few methodologies, however, report the formation of biopolymer coatings around porous nanoparticles for internal targeted drug delivery. The physiologically abundant enzyme amylase would degrade the amylose coat and initiate drug delivery appropriate for cases of dysphagia and pancreatitis.

Herein we report initial findings and characterizations of an MCM-41 drug delivery system capable of uptake and sustained release of fluorescein, mediated by concentration gradient and pH dependent electrostatics. Amylose displayed unsuitable surface interactions with bare MCM-41, yielding insufficient pore coverage. Covalent surface functionalization with trimethylsilanes improved nonpolar interactions, yet noncovalent amylose coating and enzyme promoted fluorescein release proved elusive. General outcomes and suitable next steps are presented.

TABLE OF CONTENTS

LIST OF FIGURES

LIST OF TABLES

LIST OF ABBREVIATIONS

Barrett-Joyner-Halenda	BJH
Brunauer-Emmett-Teller	BET
Cetrimonium Bromide	CTAB
Cytochrome P450	CYP
Dimethyl Sulfoxide	DMSO
Drug Delivery System	DDS
Enhanced Permeability and Retention	EPR
Hexamethyldisilazane	HMDS
Human Serum Albumin	HSA
Infra-red Spectroscopy	IR-Spec
Mesoporous Silica Nanoparticle	MSN
Mobil Composition of Matter 41	MCM-41
Non-steroid Anti-inflammatory Drug	NSAID
Phosphate Buffered Saline	PBS
Scanning Electron Microscopy	SEM
Tetraethyl Orthosilicate	TEOS
Thermal Gravimetric Analysis	TGA
Transmission Electron Microscopy	TEM
Ultraviolet-Visual	Uv/Vis
Waste Water Treatment Plants	WWTPs

ACKNOWLEDGMENTS

I would like to thank and acknowledge Dr. Brian Trewyn and all of the CSM Trewyn research group. Special thanks to Nolan Kovach, Glory Russell-Parks, and Piper McKee for their support and reviews.

To my Hanna, for her love and patience.

And to my Mom and Dad, for their support.

For from Him and through Him and for Him are all things.

To Him be the glory forever! Amen.

Romans 11:36

CHAPTER 1
INTRODUCTION AND BACKGROUND

Orally consumed medications face a steep battle for bioavailability in human systems. Bioavailability refers to the extent a substance is accessible to its intended biological destination– many obstacles stand in the way of ingested therapeutics reaching the target site.[1] Obstacles occur through the absorbance, distribution, metabolism, and excretion stages of pharmacokinetics, which describes the passage of pharmaceutics into, through, and out of the body.[17]

1.1 Barriers to Bioavailability

Following ingestion, medicine needs to be absorbed into the bloodstream. Barriers to absorption include natural digestive processes, like the harsh acidic and enzymatic conditions of the stomach, which have the potential to degrade drug molecules. After passing the stomach, medicinals may struggle to be taken in by the small intestine. Intestinal travel time and absorbance rates vary based on polarity and solubility, altering the mechanism of absorbtion.[18] This affects digestion time and somatic distribution, and must be considered and balanced when engineering a drug. Modifications made to improve potency may hinder absorbance, bioavailability, and overall treatment effectiveness.

Once absorbed, distributing the active drug through the body is complicated by other species present in the bloodstream, such as various blood proteins that freely traveling pharmaceuticals may interact with, reducing the amount of active drug available. A common clinical example is the interaction between the blood thinner Warfarin and the albumin protein in blood. Warfarin is prone to reversibly bind with human serum albumin (HSA), preventing its interaction with the target site. HSA is the main plasma carrier protein for many types of organic ligands, which compete with Warfarin for binding. When other ligands are introduced into the blood (from common foods such as peppers), bound

Warfarin undergoes competitive dissociation as new ligands interact with HSA. Warfarin in blood experiences near complete protein binding, so even a small dissociation from HSA drastically elevates circulatory Warfarin concentration.[1,19] HSA concentration also varies over time and between individuals, further fluctuating bioavailability. Erratic drug concentration is a broad problem in medicine administration which complicates properly dosing oral medications. There is a range of plasma drug concentration where therapeutic effect is maximized. Concentration above this range produces adverse effects, while subtherapeutic concentration leads to compromised treatment effectiveness.[20] Therefore, to maximize medication effectiveness, there is a desire to stabilize drug concentration and protect therapeutics from interactions within the body.

Aside from interactions with nearby compounds in blood, circulating therapeutics quickly face metabolic degradation and clearance known as the "first pass" metabolism. The first pass effect primarily involves hepatic breakdown and renal clearance, but any metabolically active tissue in the body contributes to this effect, such as the lungs and GI tract.[21] The culprit behind this phenomenon is usually a hemeprotein of the cytochrome P450 (CYP) family. CYP proteins account for the metabolic decay of 80% of common prescription drugs used today.[22] These ubiquitous proteins may metabolize multiple ingested drugs in a similar way, raising the risk of undesirable drug-drug interactions. If a drug inhibits the CYP family, this lowers the first pass effect, and increases the concentration of any other drugs taken, resulting in toxicity. Similarly, if a drug promotes a CYP pathway, it may further metabolize other drugs, leading to subtherapeutic levels and treatment failure.[23] Quantifying and combating how cytochrome P450 and the first pass effect lower medication bioavailability is difficult and depends on the specific individual and drug chemistry.[24] The body is designed to reject xenobiotic compounds, and does not distinguish if foreign compounds are actually beneficial to treat an ailment. To protect against foreign toxins, medications are opposed by the body throughout the pharmacokinetic process.

1.2 Overmedication

The clinical repartee to the body's medication intolerance has been to increase the dosage of medications. This allows a percentage of the treatment to be inactivated by digestive processes while still leaving enough active to reach the target site and achieve therapeutic effect. Dosage is correlated to bioavailability; the lower the bioavailability, the higher the dosage needed.[1] There are three major consequences to this methodology. First, heightened dosages cause more chemical exposure to non-target sites in the body, triggering adverse effects and toxicity. One such example is common over-the-counter non-steroid anti-inflammatory drugs (NSAIDs), such as ibuprofen or acetaminophen. NSAIDs are well digested and absorbed and have high initial bioavailability. Despite this, greater dosages are still required as during circulation they strongly bind to plasma proteins and are subject to heavy first pass metabolism, especially in the liver.[25] Bioavailability is quickly reduced by hepatic processes and renal clearance. This pattern of exposure correlates to the side effects of sustained NSAID use– liver and kidney damage.[25] In addition to side effects, non-target site exposure renders many potential treatments (particularly chemotherapies) unusable altogether, as the dose required to reach a cancerous tissue with sufficient bioavailability is damaging to surrounding tissues and organelles. Common chemo medicines target quickly reproducing cells to stunt the unregulated growth of cancer. The nonspecificity of this method also poisons other quickly reproducing cells, such as hair follicles, white blood cells, and cells of the stomach lining. Damage to these types of cells cause hair loss and other symptoms common to chemotherapy.[26-27] It is for this reason that the FDA rejects over 91% of submitted cancer treatments.[28] Potentially effective anticancer agents are unusable with traditional dosage requirements and administration methods.

The second issue with increased dosages are the unforeseen environmental impacts. The bulk of all consumed pharmaceuticals reach wastewater within 24 hours of consumption.[29] Wastewater treatment plants (WWTPs) strive to remove these compounds from potable water and runoff to avoid human and/or environmental exposure. Biologically active

metabolites pose particular concern, as after passing from the system, they may accumulate in bodies of water near WWTPs, affecting local wildlife. For example, ubiquitous use of oral birth control medication in the United States leads to active estrogenic derivatives reaching environmental freshwater. Anthropogenic alkylphenol derivatives have been recorded in the Mississippi River, the Great Lakes, and in several areas downstream of WWTPs in Boulder, CO.[30-32] These contaminants have biological effects on neighboring ecosystems. A species of flathead minnow's embryonic exposure to estrogenic waste lead to a high rate of demasculinization in flatheads downstream of Boulder WWTPs.[30-31] Demasculinization threatens the reproduction of the species and the local food chain. The environmental impact of high-dosage birth control medications serves as a canary-in-the-coal-mine for the environmental toil of overmedication as a whole.

Finally, overmedication imposes unnecessary costs. Increased dosages means more active molecules, and higher prices for researchers, government aid, and consumers. The high price of consumer pharmaceuticals is a prevalent issue in American politics; the average American spent $1300 on prescription medication in 2021 alone.[33-34] Ineffective medication administration and high dosages contribute to the high price of consumer medications.

1.3 Drug Delivery System

Traditional drug delivery methods are unable to alleviate the challenges associated with drug administration. Even intravenous treatment, while avoiding digestion and absorption, is subject to the first pass effect, full body circulation, and non-target site exposure. In addition to the continual development of novel drugs, it is equally or more important to consider new methods to use traditional drugs with higher efficiency.[3] A nanocarrier capable of encapsulating medication until it reaches the target site would enhance local bioavailability while lowering non-target site exposure and toxicity. Fragile treatments like DNA, RNA, or protein therapy denature during digestive processes and transit– a DDS could allow their preservation and efficacy. High surface area porous materials have been

applied towards this end in literature. Mesoporous silica nanoparticles (MSN) have received particular interest in this ever since the Vallet–Regí group proposed their novel application as DDSs for the first time in 2001.[35]

MSN are a class of porous nanoparticles made from amorphous silicon dioxide assembled in an ordered framework. In MSN, impressive surface area and pore volume, nontoxic nature and biological safety, thermal and chemical stability, and immense modification potential combine to form a promising avenue towards controlled drug delivery.[2-7] MSNs routinely display surface areas over 1,000 m^2/g. This is a crucial characteristic in a DDS, as cargo loading into pores is a surface phenomenon, mediated by drug/surface interactions. Roughly 99% of the MSN's surface is internal– vast pore interiors can host and interact with a variety of drug and biomolecule cargo.[3] This has been exploited to achieve particle loading into MSN as high as 35% by weight.[36]

Any material with clinical aspirations needs to be biologically safe and compatible. Unaugmented MSNs are composed exclusively of silica, which has been classified as safe by the FDA for over 50 years.[37] Therefore, MSN pose no biological threat from a chemical perspective. Nanomaterials often behave differently than their bulk counterparts, however, and MSN may uniquely interact with living systems. Consequently, many studies are investigating the *in vivo* pharmacokinetic pathway of MSN materials. Overall, unadulterated MSNs clear renally from the body without much retention. Studies found nearly all ingested MSN is excreted within 96 hours.[37] Prior to clearance, the biodistribution of MSN has been probed in rats and mice, finding that MSN accumulation occurs minorly in the lungs, liver, and spleen, but factors such as retention/circulation time and accumulation sites vary greatly depending on what modifications have been performed on the nanoparticle.[38-39] Overall, minor MSN accumulation did not accompany any adverse effects. Preliminary health studies suggest the fast clearance and chemical inertness of MSN makes it a fine candidate for DDSs.

Nanocarriers applied to the body must be chemically robust to survive the journey and prevent loaded cargo from premature leaching. The *in vitro* degradation path of MSNs in physiological conditions has been studied; the silica framework intrinsically allows MSN to remain stable long enough for use as a DDS.[40] Si-O bonds are strong (bond enthalpy 450 kJ/mol); the silica lattice composing MSNs is robust and stable in physiological conditions.[41] The main degradation pathway of MSNs is hydrolysis of the Si-O bonds, resulting from nucleophilic attack of aqueous hydroxyls. This breakdown produces free silica (in the form of silicic acid), which as mentioned, is nontoxic to human systems and FDA approved.[37]

The modification potential of MSNs also arises from the chemistry of the Si-O bond. On the material's surface, the Si-O lattice terminates in Si-OH moieties called silanol groups. The electron withdrawing nature of the silicon in the Si-O bond leads to an especially electronegative oxygen atom in the silanol.[30] Therefore, the silanol OH group is particularly acidic and responsive to chemical modification; altering the internal or external surface of MSN is achievable through reactions with the exposed silanols. Covalent condensations with commercially available functionalized siloxanes allow the addition of various chemical moieties and properties, such as basic amino sites.[42-44] This allows drug uptake, storage, and release to be tuned specifically for the drug in question, as cargo adsorption into the material's pores is a surface phenomenon strongly influenced by pore/cargo interactions.[3] The MSN surface can also be tailored to promote different biological interactions and chemical properties, such as altering polarity or charge to promote certain chemical interactions, absorption pathways, or targeting in the body.[35] Potential for specific fine tuning of the material makes MSN a versatile candidate for use in a DDS.

Of all the MSN type materials exploited for a DDS, one is prevalent in literature: Mobil-Composition-of-Matter-41. MCM-41 is a spherical nanoparticle with a honeycomb-like distribution of cylindrical pores. It was first developed by the namesake company ExxonMobil in 1993 for use in crude oil separations.[46] Soon after, MCM-41

became one of the most prominent materials used for DDSs for the aforementioned benefits of MSN, and for the desirable pore sizing and synthetic pathway of MCM-41 specifically.

By definition, MSNs have pores broadly ranging from 2-50 nm in diameter; MCM-41 has consistent repeating pores averaging about 3 nm in diameter.[35-37] While tuneable, this starting point is appropriate for delivery of existing pharmaceuticals. Ibuprofen, for example, is roughly 1.3 nm in length. Diffusion through the pores of MCM-41 is correlated to pore and drug size; the pores are 2-3 times the size of many drugs, allowing sufficient room for diffusion, while still having a close enough space for drug/pore surface interactions.[5]

Further, MCM-41 has a well understood and simple to perform synthesis known as a bottom-up liquid-crystal surfactant assembly. The nanoparticles get their characteristic pore distribution from the liquid-crystal morphology of surfactant molecules in an aqueous solution. Polar/nonpolar interactions drive long chain surfactant molecules to form micellar rods, which then self assemble into hexagonal arrays. A silica precursor is then added, which undergoes base catalyzed hydrolysis and condensation around the micelle template. This forms a layer of silica encapsulating the surfactant liquid crystals. After the template is removed by acidic extraction or calcination, the silica nanoparticles are left with vacant cylindrical pores, in the same hexagonal array as the template.[47-49] This procedure is conducive to modifications– introducing various nonpolar chemicals into the hydrophobic center of the pore-forming-micelles, or increasing the surfactant's carbon chain length causes an increase of the micelle diameter, and thus, the final MCM-41 material displays larger pores, up to roughly 8 nm in diameter.[7,50-51] This accommodates larger biomolecule payloads such as proteins.[42] During synthesis, various metals can be doped into the silica framework, altering the material's electronic properties. For example, the different valency of aluminum can increase the materials Lewis acidity and promote different electronic interactions.[52-53] Further, by delaying the surfactant extraction and clearance of pores, the aforementioned silanol modifications can occur only on the external

surface, providing different chemical environments on the inside or outside of the material. Surface tailorability, simple synthesis, and appropriate pore sizing makes MCM-41 ideal for drug delivery.

1.4 MCM-41 as a Delivery Vehicle

MCM-41's potential has led many research groups across current literature to charge its pores with active drug molecules with poor bioavailability to increase efficacy with an improved DDS.[8-10] One such drug explored is the commercial prostate cancer treatment bicalutamide– a drug with poor aqueous solubility and intestinal absorption, and thus low oral bioavailability. Consequently, bicalutamide treatments involve more frequent doses and lower patient compliance.[9] Pharmaceutical attempts to chemically increase the drug's solubility also increased its retention and undesired accumulation, leading to adverse effects.[54] In 2021, Popova et al. sought to improve bicalutamide's bioavailability without altering the drug itself.[9] Several MCM-41 systems were used for drug uptake and release in simulated media and living cells, in an effort to transfer the insoluble drug into circulation through a soluble MCM-41 DDS. The pores were charged with a therapeutic level of the cancer treatment, which diffused back out under physiological conditions over the course of 12 hours. MCM-41 provided sustained bicalutamide release overtime, reducing the initial burst and crash of bioavailability custom for oral medications, and leading to a significant improvement of the *in vitro* anticancer activity.[9] Controlled release and concentration stabilization benefit oral medication as a whole, but is broadly promising for other cancer treatments. DDSs can "passively target" cancerous tissue by sustained release and accumulation through the enhanced permeability and retention (EPR) effect. Nanoparticles gather in cancerous tissues faster than they do in healthy tissues, due to the great oxidative need and thus vascular connectivity of tumors.[55-56] In this way, nanoparticle accumulation can reduce the amount of drug in active circulation, and increase drug concentration directly at the target site, lowering toxicity and improving treatment effectiveness.[4,56-57]

Beyond sustained release, there exists a desire for a DDS to "actively target" a discrete portion of the body– to tailor treatment towards specific ailments and biochemical environments. To achieve this, "gatekeepers" can be utilized with stimulus responsiveness. A gatekeeper material should block the pores of the MCM-41 after the drug is loaded, allowing zero therapeutic release prior to reaching the target, after which the gatekeeper would breakdown or otherwise alter, restoring access to the pores and beginning release of the therapeutic.[10-13] This provides a binary on/off release, where the therapeutic is withheld until reaching a specific stimulus typical of the treated pathology. The MSN should respond to a chemical variation present in the diseased tissue, but not in a healthy tissue/organ. Internal stimuli suitable for targeting include pH, which varies between the extracellular matrices of cancerous and healthy tissues, or the dysregulation (be it under or overexpression) of certain enzymes and/or antibodies that occurs in tissues suffering from various pathologies.[2-4] There are near countless biological signals emblematic of disease states that can be used for triggering therapeutic cargo ejection from MSNs.

For a practical DDS, the choice of gatekeeper material must be considered for its biocompatibility, specificity to a biological signal, ease of synthesis and modification, economic cost, etc. Therefore, natural digestible biopolymers are of particular interest. Polysaccharides with these qualities have been widely used in biomedical fields already.[14-16,58] Alginate is a linear, anionic polysaccharide derived from brown algae, which displays excellent biocompatibility and is declared safe by the FDA for human application. The polysaccharide chain of alginate forms folded spiral structures that can ionically crosslink in the presence of divalent metals, like Ca^{2+}, forming three-dimensional net structures and hydrogels, which are exploited in wound dressing and drug delivery.[3] This binary response has lead to alginate being covalently linked to the surface of MSN to provide Ca^{2+} specific drug release, in which the formation of crosslinking blocks the pores and discourages premature release.[59-61] Conversely, chitosan is a cationic biopolymer derived from chitin, an exceedingly abundant natural polysaccharide responsible for the

shell and cartilage rigidity of arthropods. The unique amino functionalization of chitosan is chemically reactive and provides unique pH based solubility and electrostatic interactions with negatively charged molecules, such as DNA and RNA.[3,62] Covalently fixed chitosan gatekeepers have provided pH specificity for MSN delivery systems.[63-64]

A biopolymer especially relevant to the human system, however, is amylose– a nonionic linear polysaccharide composed of D-glucose monomers connected via α-1-4-glycosidic linkages. Tandem with amylopectin (which differs from amylose by additional α-1-6-glycosidic crosslinking and branching) amylose constitutes dietary starch.[3,65-66] Amylose nanoparticles have been formed in literature for a variety of biomedical applications, including biosensing and drug delivery.[13-16] The biological compatibility, relevance, sustainable sourcing, and tailorability of amylose makes it a suburb candidate for MCM-41 pore coverage, while prevalence in the human diet means that the enzyme capable of hydrolyzing amylose, amylase, is physiologically abundant, particularly in saliva, the pancreas, and the small intestine.[67-68] This biological distribution provides an avenue towards site selective drug delivery. An amylose coated DDS would initiate therapeutic release when dissolved orally, providing medication administration for those unable to swallow pills due to dysphagia. With this avenue, medicine can access the bloodstream directly through the vascular connectivities of the oral mucosa, bypassing digestion and lowering the first pass effect. Further, vastly elevated amylase concentration is indicative of pancreatitis, a condition arising from pancreatic inflammation, leaching of dietary enzymes, and painful self digestion.[69-70] The cause of the malady could be used as a specific target to direct the delivery and local release of antibiotic agents directly at the affected portion of the GI tract.

1.5 Hypothesis/Specific Aims

Combining the aforementioned rationale, we propose a delivery vehicle synthesized from an MCM-41 mesoporous silica support with a natural biopolymer coating will selectively release drug molecules only upon digestive enzyme catalyzed hydrolysis of the polymer.

Long term application includes antibiotic drug administration in amylase-rich environments that surround intestinal cells in individuals suffering from pancreatitis.

In this pursuit, we are targeting several knowledge gaps with broad application. To the best of our knowledge, a non-covalently linked amylose coated MCM-41 DDS has not been shown in literature; amylase mediated active targeting is novel in MSN drug delivery. Further, the methodology pursued to form a noncovalent biopolymer coating on biomedical nanoparticles will have broad application in diagnosis and drug delivery.

CHAPTER 2
MATERIALS AND METHODS

All purchased materials were used as received unless specified otherwise. General procedures are outlined below. Minor alterations may have been made and specified in *Appendix A.1.*

2.1 Materials

Hexadecyltrimethylammonium bromide 99%, tetraethyl orthosilicate 99.0%, sodium hydroxide 98%, anhydrous dimethyl sulfoxide 99.0%, concentrated aqueous ammonia (approx. 14.5 M), concentrated hydrochloric acid (37% w/w), sodium phosphate dibasic 98%, potassium phosphate monobasic 98.0%, sodium chloride 98.0%, potassium chloride 98.0%, calcium chloride 93%, fluorescein powder (free acid), α-amylase from Aspergillus Oryzae (approx. 30 U/mg), amylopectin from potato starch, Lugol's iodine/potassium iodide solution, and dry hexamethyldisilazane were all purchased from Sigma Aldrich. USP/NF grade ethanol, methanol, and ACS grade hexanes were purchased from Pharmco-Aaper. Amylose from potato 98% was purchased from City Chemical. Nanopure water was obtained using a Thermo Scientific Barnstead E-Pure water purifier. Phosphate buffered saline (PBS, 100 mM) was prepared by combining 8.00 g NaCl, 0.20 g KCl, 1.78 g sodium phosphate dibasic, and 0.24 g potassium phosphate monobasic in one liter of nanopure water. The pH was measured with a pH probe and set to the desired value by adding dilute HCl and NaOH as needed.

2.2 MCM-41 Synthesis

MCM-41 was synthesized using a bottom-up liquid crystal surfactant assembly, followed by an acidic extraction to remove the organic surfactant and empty the pores. 1.00 g of CTAB was dissolved in 480 mL of nanopure water with 4.0 mL 2.0 M sodium hydroxide to

form a 2.1 mM CTAB solution. The mixture was heated and stirred vigorously for 60 minutes at 80° C. 6.0 mL of TEOS was then added dropwise over the course of 5 minutes. The reaction mixture continued to stir vigorously at 80° C for an additional 75 minutes, then cooled to room temperature. The mixture was vacuum filtered to collect a white gel which was washed with copious amounts of nanopure water and methanol. The white gel was air dried overnight, yielding a fine white powder. The powder underwent acid extraction by stirring vigorously for 120 minutes at 68° C in acidic ethanol (150 mL of ethanol and 2.0 mL of 12.1M (37w%) HCl for every 1 gram of MCM-41). The solution was then cooled to room temperature and vacuum filtered. The particles were washed with ethanol, then water, then methanol, and allowed to air dry overnight to obtain usable MCM-41 with unblocked pores.

2.3 Stöber Silica Synthesis

Nonporous silica nanoparticles were synthesized for use in control studies. In general, 150 mL ethanol and 40 mL of concentrated ammonium hydroxide (14.5M), were combined in a round bottom flask and stirred at 400 rpm and 65° C for 15 minutes, after which, 10.0 mL TEOS was added dropwise over the course of 5 minutes. The reaction continued at the same heat and stir rate for two hours, and then was cooled to room temperature, vacuum filtered, and rinsed copiously with methanol to collect the Stöber silica particles, which were air dried overnight.

2.4 Fluorescein Loading

In general, 100 mg of MCM-41 was combined with 40 mL PBS solution (with a fluorescein concentration of 50. µM in a 100 mM PBS at pH 3.0). The solution was sonicated for 5 minutes before being stirred vigorously at room temperature for 24 h. After settling, an aliquot was taken for Uv/Vis analysis to compare the fluorescein concentration before and after loading. Fluorescein uptake was quantified using a premade calibration curve, ranging from 2-20 µM. The fluorescein loaded particles were collected by

centrifugation at 3000 G for 10 min (24° C) and dried in a lab oven at 70° C. The procedure was repeated with the same amount of Stöber silica substituted for MCM-41 for the loading procedure control.

2.5 Biopolymer Coating

Separate amylose and amylopectin solutions (concentrations of 1 or 2% by weight) were made with a mixture of 90:10 dimethylsulfoxide:water and the same fluorescein concentration used for loading. These solutions were refluxed at 80° C and stirred at 300 rpm for two hours, at which point, the solutions were entirely transparent, showing complete dissolution of the respective biopolymers. To coat the fluorescein loaded MCM-41, 100 mg of loaded MCM-41 was combined with 10 mL of the desired concentration/biopolymer solution, and was sonicated for 5 minutes to dissolve the MCM-41. Approximately 25 mL of methanol was added rapidly to precipitate the biopolymer around the loaded MCM-41. To remove large conglomerates, the mixture was centrifuged at 1200 G for 10 min (24° C). The supernatant was decanted and the particles were rinsed with methanol to remove residual DMSO. The particles were then freeze dried, and stored in vacuum overnight.

2.6 Fluorescein Release

In general, 5-6 mg of the desired loaded particle was dissolved in 10.0 mL of 7.4 PBS. The solution was stirred at 250 rpm with measurements being taken every 30-60 minutes. To take a measurement, the stirring was stopped and the solution settled for 5 minutes to allow the contents to collect on the bottom. A top portion of the mixture was then drawn with a pipette and charged into a cuvette for analysis with a Vernier fluorescence/UV-Vis spectrophotometer at a wavelength of 490.2 nm. Absorbance measurements were recorded in triplicate and averaged. Following measurement, the aliquot was returned to the reaction flask and the flask resumed stirring. In the case of amylose coated particles, the release solution was made to have an amylase concentration of around 0.5 mg/ml and a

calcium dichloride concentration of 2 mM. The amylase's absorbance was accounted for via calibration.

2.7 HMDS Functionalization

To introduce the trimethylsilane surface functionalization, previously prepared MCM-41 was reacted with hexamethyldisilazane. 250 mg of MCM-41 was combined with 25 mL of hexanes and 0.5 mL of dry HMDS (concentration 2.4 mM) in a round bottom flask; the solution was allowed to reflux at 60° C for 24 hours. The reaction was then cooled, vacuum filtered, and rinsed with copious amounts of hexanes before drying in a lab oven.

2.8 Nitrogen Physisorption

The reported nitrogen adsorption/desorption measurements were carried out using a Micromeritics TriStar II surface area and porosity analyzer. For each measurement, roughly 100 mg of sample was degassed under nitrogen at 80° C for 4 h, then the isotherm was generated by supplying nitrogen gas at -196° C and quantifying the deviation of pressure in the sample chamber compared to a reverse chamber, resulting from adsorbate gas leaving the gas phase and adhering to the material's surface. Barrett-Joyner-Halenda and Brauner-Emmett-Teller mathematical models were used to calculate surface area and porosity data from the generated isotherms. The Langmuir model was used for non-mesoporous calculations.

2.9 Thermal Gravimetric Analysis

8-12 mg of a given sample was placed on a ceramic pan and thermogravimetric analysis was conducted with a TA TGA Q500 instrument. The sample was heated from room temperature to 800° C at a rate of 13° C min^{-1} with a balance and sample flow of nitrogen at 20 mL min^{-1}. Weight loss before 100° C was attributed to solvent and adhered water evaporation and was discounted from any calculations.

2.10 Infra-red Spectroscopy

IR spectroscopy was performed by placing approximately 5 mg of dry sample on the sample deck of a Thermo Electron Nicolet 4700 FT-IR spectrometer and collecting the transmittance spectrum after running an open air background measurement.

2.11 Electron Microscopy

SEM images were taken with a AMRAY 3300 field emission scanning electron microscope. Parameters such as working distance, voltage, etc. were all varied per sample to obtain the clearest image. The parameter specifics are shown below each SEM photograph. Silica is poorly conductive, and thus gold sputtering was performed during sample prep to obtain higher resolution images.

CHAPTER 3

RESULTS AND DISCUSSION

3.1 Silica Characterization

Conventional MCM-41 of good quality was successfully synthesized. Nonporous Stöber silica was also synthesized to use as a negative control and confirm that the drug delivery properties displayed by MCM-41 were due to the mesopores and not simple surface adhesion. SEM was used to confirm the formation of nanoparticles, rather than bulk material. It can be observed in the SEM images that both materials formed succinct spherical particles of consistent morphology. The MCM-41 particles appeared to be smaller than the Stöber silica, and were thus difficult to image with suitable clarity (the image of the MCM-41 is shown in *Appendix A.2.1*). MCM-41 roughly averaged 100 nm in diameter, while the Stöber silica was around 250 nm in average diameter. The Stöber silica had a less consistent distribution of particle sizes. While MCM-41 appeared to be uniform in size, Stöber silica had some smaller particles present as well. This is to be expected, as in the absence of a structure directing agent, Stöber silica is more prone to different sizing, while the MCM-41's morphology is dictated by the liquid crystal assembly.

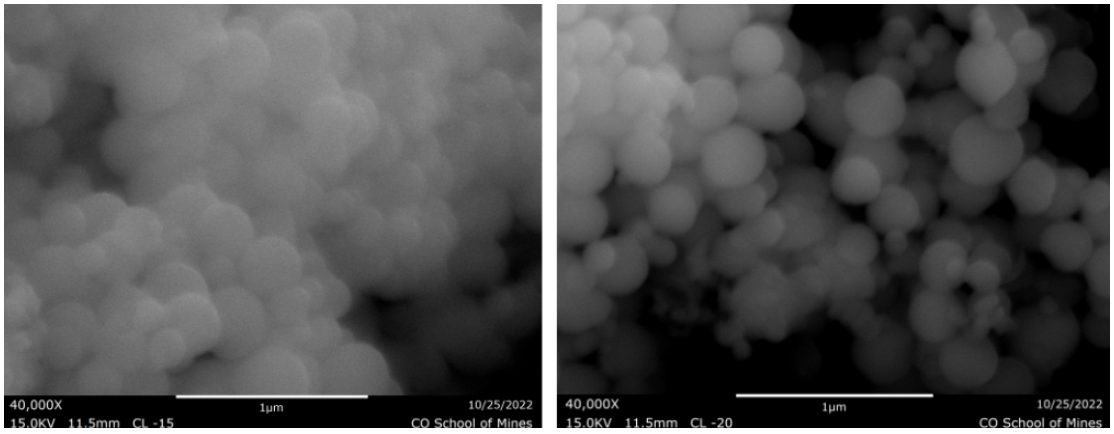

Figure 3.1 SEM images of Stöber silica, showing succinct nanoparticle formation and largely consistent morphology.

Overall, electron microscopy suggested both nanoparticles formed succinctly, not as a bulk conglomerate. Characterization by nitrogen physisorption yielded expected results for both material types. The MCM-41 displayed an IUPAC classified type IV isotherm, emblematic of a mesoporous material.[71] Initial uptake arose from the material's surface being coated with an adsorbate monolayer, while at a relative pressure of around 0.3, steep uptake occurred, representing filling of the mesopores. At this point, a hysteresis loop was observed between the adsorption and desorption branches, characteristic of the different mechanisms by which gas fills and empties the mesopores. Stöber silica generated a type III isotherm, with no significant uptake nor hysteresis loop (the Stöber silica isotherm can be seen more clearly in *Appendix A.2.3*). This data is consistent for a nonporous material, displaying poor gas/surface interaction. The BET mathematical model was used to calculate the surface area of the mesoporous MCM-41, which was between 1,000-1,100 m^2/g for each sample. BET modeling is accurate only for pores from 2-50 nm and thus insufficient for analyzing nonporous Stöber silica. Therefore, Langmuir modeling was used to determine the Stöber silica surface area, which was calculated to be 11 m^2/g, drastically less than the porous counterpart and consistent for a nonporous material. The BJH pore distribution model was used to analyze pore volume based on diameter. This showed uniform monodisperse pores of around 2.5-3.0 nm for the case of MCM-41, consistent to literature. Stöber silica was again confirmed to be nonporous.

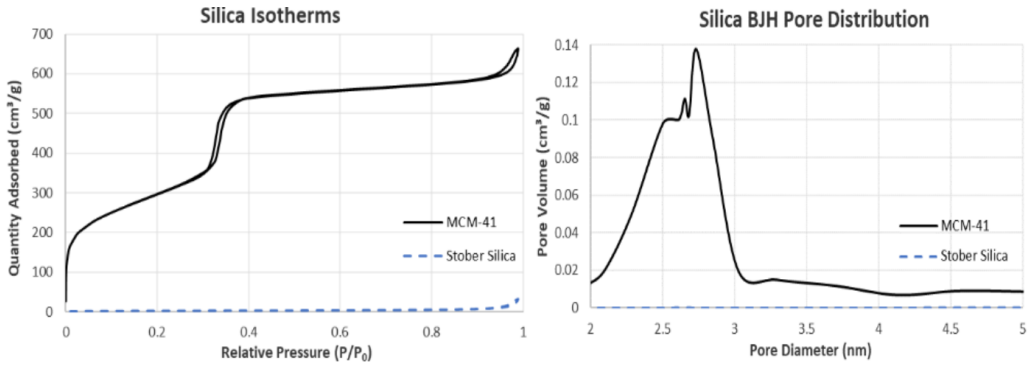

Figure 3.2 Nitrogen physisorption isotherms for MCM-41 and Stöber silica. Mesoporous MCM-41 displays a type IV isotherm; nonporous Stöber silica a type III.

TGA was performed to show the successful clearance of the organic surfactant from the MCM-41 pores. Weight loss occurring prior to 100° C is attributed to adhered moisture evaporation and is discounted from comparisons. Between 100-800° C, the MCM-41 only showed 6.9% weight loss, which can mostly be attributed to surface silanol condensation. The surfactant CTAB is known to have a sharp TGA degradation point at 240° C.[72] MCM-41 had no sharp degradation in this range, suggesting the complete clearance of surfactant from the pores. Stöber silica showed minor weight loss of 8.2%, with no significant points of weight loss. This value is similar to the MCM-41 and expected for a pure silica material.

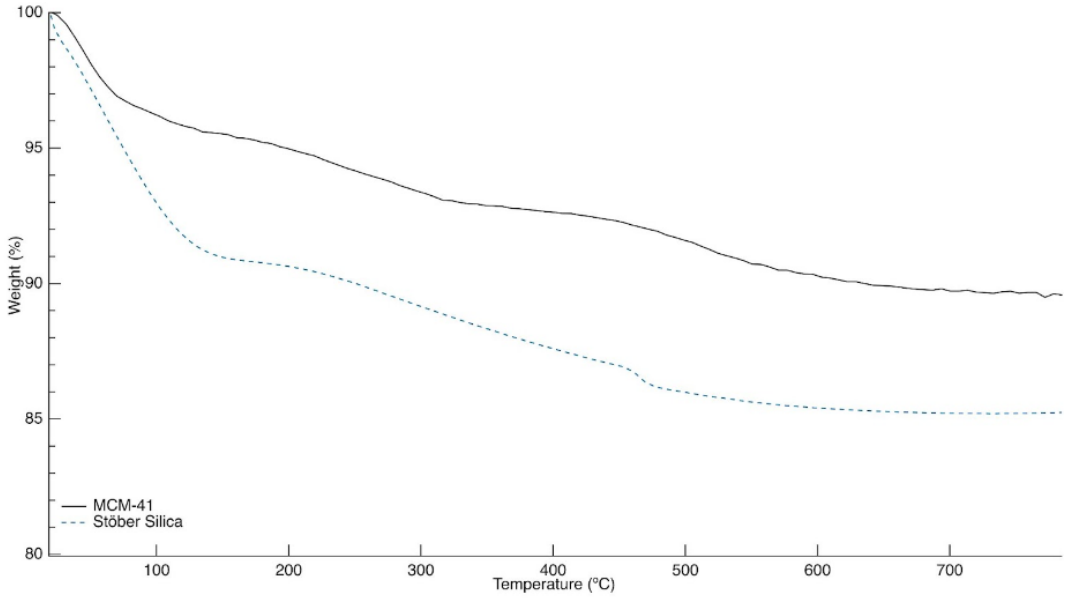

Figure 3.3 TGA plot for MCM-41 and Stöber silica, mass loss attributed to silanol condensation. No degradation occurring from organic surfactant.

3.2 Fluorescein Loading and Release

Fluorescein was selected for use as a drug analog because of its appropriate molecular size (comparable to common pharmaceuticals) and prominent light absorbance at 490.2 nm, allowing for qualitative analysis visually and quantitative analysis by Uv/Vis spectroscopy. Fluorescein was loaded into the pores of MCM-41 via solvent impregnation

at various concentrations and pHs. The quantity of fluorescein loaded was measured by Uv/Vis spectroscopy and a previously prepared calibration curve. Loading was dictated by both concentration gradient and pore/surface interactions. It was observed that higher concentrations of loading solution lead to higher loading percentage, up to the solubility limit of fluorescein. Further, loading percentage drastically increased at lower pH values. This can be explained by static repulsion that prevents favorable drug/pore interactions and limits uptake. The surface silanols of silica and the hydroxyl group of fluorescein are weakly acidic, and thus negatively charged at a neutral pH. At lower pH values, protonation is more favorable, and both species become neutral and no longer repel. pH 3.0 showed the highest loading. At this point, the solution is well below the isoelectric point of MCM-41 and pKa of fluorescein (approximately 5.5 and 6.4, respectively).[73-75] At pH 3.0, the MCM-41 was able to adsorb 95% of the fluorescein from solution into the pores, compared to as low as 55% at neutral pH.

Table 3.1 pH dependant fluorescein uptake.

	pH 3	pH 5	pH 7
Loading %	95	64	55
Weight %	0.6	0.4	0.3

Loading efficiency of 95% of the available fluorescein was achieved when concentration was maximized to a level that prevented the poorly soluble fluorescein from precipitating out of solution (saturation and limited solubility occurred at concentrations above 50. µM). To further increase loading quantity, the volume of loading solution was doubled. After doing so, the loading percent was still determined to be upwards of 95%. The quantity of fluorescein adsorbed into the pores of MCM-41 nearly doubled; the limit to cargo loading was the amount of fluorescein available in solution. Higher volume solvent impregnation corresponded to loading efficiency of 0.6% by weight (fluorescein weight out of total loaded MCM-41 weight). The acidic loading solution allowed elevated loading percentages. For drug delivery, this suggests that higher loading can be achieved by varying the loading

parameters and considering surface/drug interactions.

The loaded samples were subjected to nitrogen physisorption to quantify surface area reduction caused from fluorescein occupying the pores. Duplicate samples "Load-1" and "Load-2" were prepared according to the standard loading procedure at pH 3.0. The parent MCM-41 of these loadings had a BET surface area of 1,070 m^2/g, while Load-1 and Load-2 had reduced surface areas of 930 and 860 m^2/g, respectively. Both samples showed type IV isotherms and retained mesoporosity, with reduced pore volume and surface area as fluorescein now occupied the pores. Qualitatively, the volume reductions were consistent with Uv/Vis fluorescein uptake analysis. Load-1 and Load-2 absorbed 95% and 94% of the fluorescein from the loading solution, corresponding to the loaded MCM-41 being 0.6% fluorescein by weight. The load percentages are within expected imprecision of the spectrophotometer, and not statistically different between the two trials.

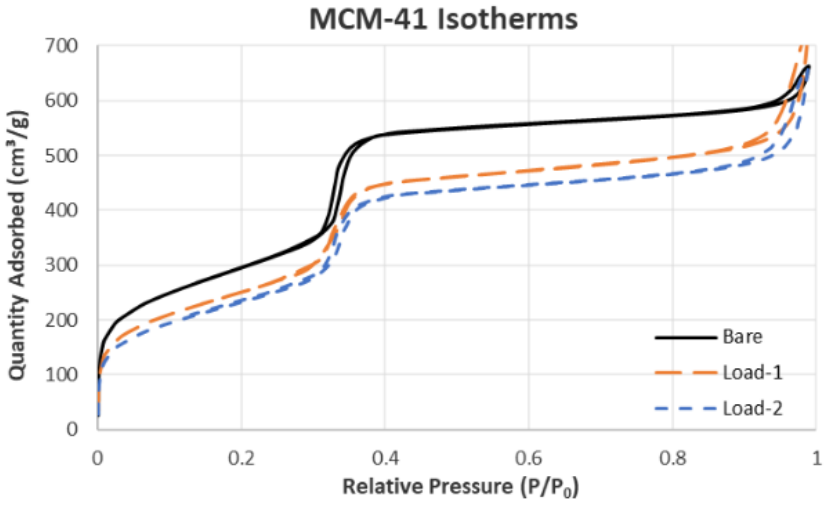

Figure 3.4 Isotherms for bare and loaded MCM-41, each displaying a type IV isotherm. Decrease in surface area due to fluorescein pore occupation.

Fluorescein release studies were conducted for various loaded MCM-41 samples. Primarily, it was seen that after transferring dry loaded MCM-41 to fresh PBS, only MCM-41 would release fluorescein out; Stöber silica was unable to uptake or release fluorescein. Further, release kinetics were dictated by loading amount. Samples with lower

loading amounts provided more sustained release, while concentrated low pH loadings had more of a burst effect, as the high amount of fluorescein in the pores was protonated in the release buffer and quickly vacated from the pores. As a drug delivery system, this demonstrates how surface interactions can dictate release rates. Drugs with disfavorable interactions that repel from the pore surface can release quickly, appropriate for tumor targeting, while more favorable surface interactions and lower loading percentages can provide sustained release and improved bioavailability over time.

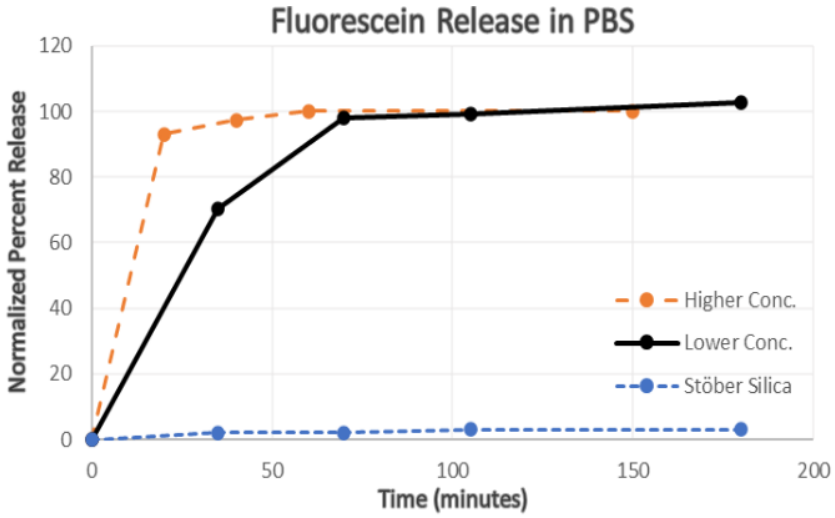

Figure 3.5 Release kinetics of fluorescein loaded silicas, determined by Uv/Vis. MCM-41 provided sustained release, while Stöber silica did not uptake nor release fluorescein.

3.3 Biopolymer Coating

To achieve enzyme specific fluorescein release, amylose and/or amylopectin were used to coat the pores of the loaded MCM-41. This was done through a variety of precipitation methods (based on literature syntheses and detailed in *Methods 2.5* and *Appendix A.1*). Two samples in particular, "Coat-1" and "Coat-2" were prepared from the same loaded MCM-41, and different amounts of amylose. To test enzymatic responsiveness, the particles underwent the aforementioned release procedure in the absence and presence of amylase. It was observed that for both cases, the particles released fluorescein regardless of

the addition of amylase. It was speculated that the enzyme may have been ineffective, and fluorescein caught in the outer portion of the starch coat provided nondescript release.

To test the effectiveness of the enzyme, a qualitative experiment was conducted with Lugol's reagent (iodine potassium iodide) as a triiodide source. Triiodide in solution forms a vibrant yellow/orange color, yet in the presence of amylose, deep purple appears. Amylose in solution forms long alpha helices, which can wrap around the triiodide complex, changing its optical properties. This reagent is sensitive to amylose concentrations in the ppm range and is useful to determine if the enzyme successfully hydrolyzed the amylose helices.[76] 3 mg portions of each attempted amylose coated MCM-41 were placed in 3 mL of 7.4 pH PBS, while only one had the presence of amylase. After one hour, a few drops of Lugol's solution were added to each mixture. The control without amylase turned deep purple, signifying the presence of amylose, while the enzymatic sample did not change color, confirming the absence of amylose and effectiveness of the enzyme (one such colorimetric study is pictured in *Appendix A.2.4*). Therefore, it was observed that the enzyme functioned properly and the amylose in the Coat-1 and Coat-2 samples was hydrolyzed, yet fluorescein release did not increase.

To further probe if the pores were covered, nitrogen physisorption was employed. Both samples maintained type IV isotherms (shown in *Fig. 3.6*) and hysteresis loops indicative of unblocked mesopores. The BJH pore distribution corroborated the preservation of monodisperse mesopores remnant of the parent material. The isotherm scale did imply a decrease in surface area, however. The BET surface area of Coat-1 and Coat-2 indeed reduced drastically from the parent MCM-41 material (to 440 and 260 m^2/g for Coat-1 and Coat-2, respectively.) In light of the nondescript release and observed porosity, this data was interpreted not as evidence of pore coverage, but as an artifact of mixing mesoporous nanoparticles with nonporous amylose particles, resulting in a decreased surface area per unit mass.

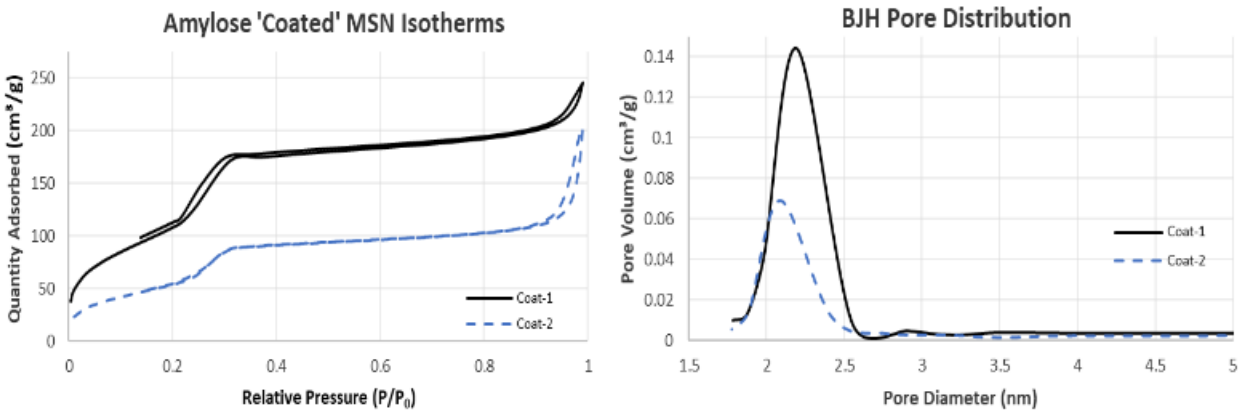

Figure 3.6 Isotherms and pore distributions of the amylose 'coated' MCM-41 samples. Both retained type IV isotherm shape and mesoporosity.

To interrogate this, TGA was conducted to quantify the weight percentage of amylose present in each sample. The TGA data was consistent with this theory. Beyond 100° C, Coat-1 displayed 27.5% mass loss, while Coat-2 (which had the lower surface area) had 63.0% mass loss. The degradation pattern of both samples were consistent with that of amylose. Literature reveals amylose undergoes minor degradation around 150-200° C, corresponding to long chain scission, and sharp degradation at 280° C, which involves the decomposition of the glucose ring.[77] The TGA data (shown in *Fig. 3.7*) reflects inflection points and heightened degradation at these values. The magnitude of weight loss qualitatively corresponds to the surface areas of these materials. Coat-1 had a higher surface area per unit mass, and less amylose present than Coat-2. This is consistent with the experimental methodology, where Coat-2 was prepared with a higher amylose amount than Coat-1.

The lack of enzymatic fluorescein release (while amylase was confirmed to be properly functioning), retention of porosity after the coating procedure, and the TGA degradation pattern and weight loss all suggested that amylose nanoparticles formed independently and did not endcap the loaded MCM-41. This conclusion was consistent for the various altered methodologies outlined in *Appendix 2.1.*

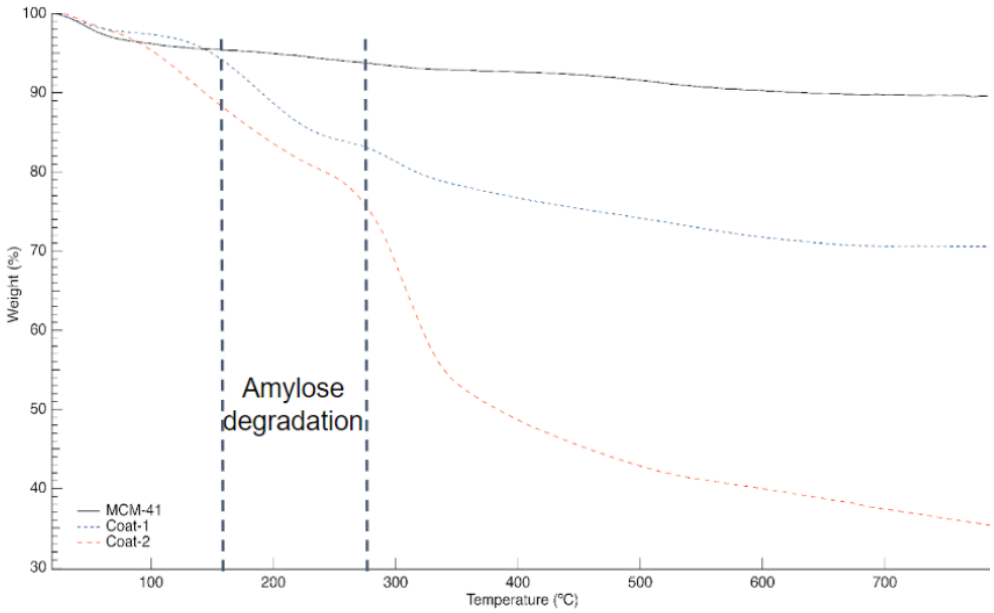

Figure 3.7 TGA data for coated MCM-41. Samples with higher amylose quantities had higher weight loss, consistent with amylose degradation temperatures.

Therefore, rather than a methodology error, poor electrostatic interactions can be attributed to this observation. As mentioned, MCM-41 is weakly acidic and displays a partial negative surface potential at neutral pH. Amylose is a nonpolar long-chain molecule that unfavorably interacts with this polar surface. In literature, amylose nanoparticles have been shown to form around nonionic surfactants, such as Tween80.[16] To promote better surface coverage, MCM-41 underwent surface modification to increase nonpolar/nonionic character and become better suited for amylose interactions.

3.4 MCM-41 Surface Functionalization

To achieve the desired surface chemistry, a trimethylsilane functionalization was selected. HMDS is commonly used in silica chemistry to institute this moiety and add hydrophobic properties to silica materials such as MSN.[78-80] Bare MCM-41 was dried in a lab oven to remove any surface adsorbed water from the silanols. Then, reaction with HMDS yielded the surface modification according to the scheme outlined in *Fig. 3.8.*

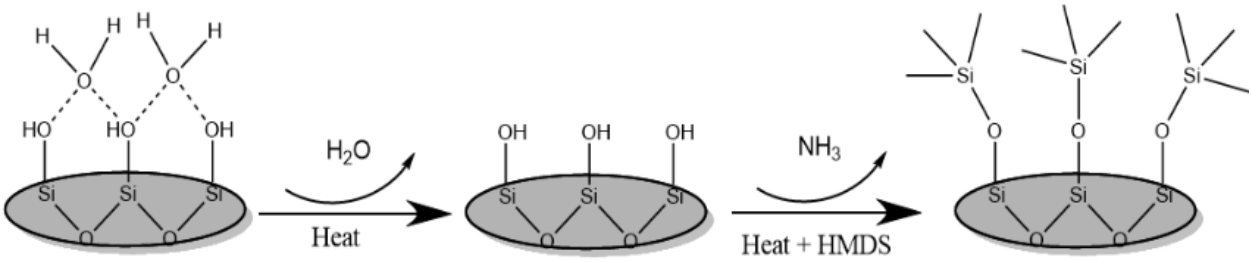

Figure 3.8 General scheme of HMDS functionalization: evaporation of surface adhered moisture and reaction with exposed silanols.

IR spectroscopy was then conducted to confirm the disappearance of the OH stretch and emergence of the trimethylsilane functionality in the HMDS augmented material (HMDS@MCM-41). The IR data was consistent for the expected carbon functionalization. Primarily, the silanol OH stretch present at 3300 cm^{-1} for the MCM-41 sample was absent following the HMDS treatment. The loss of OH signal coupled with the emergence of two peaks corresponding to C-H and Si-C bonds (2900 and 1250 cm^{-1}, respectively) is emblematic of a successful conversion of surface silanols to trimethylsilane groups.[81-82]

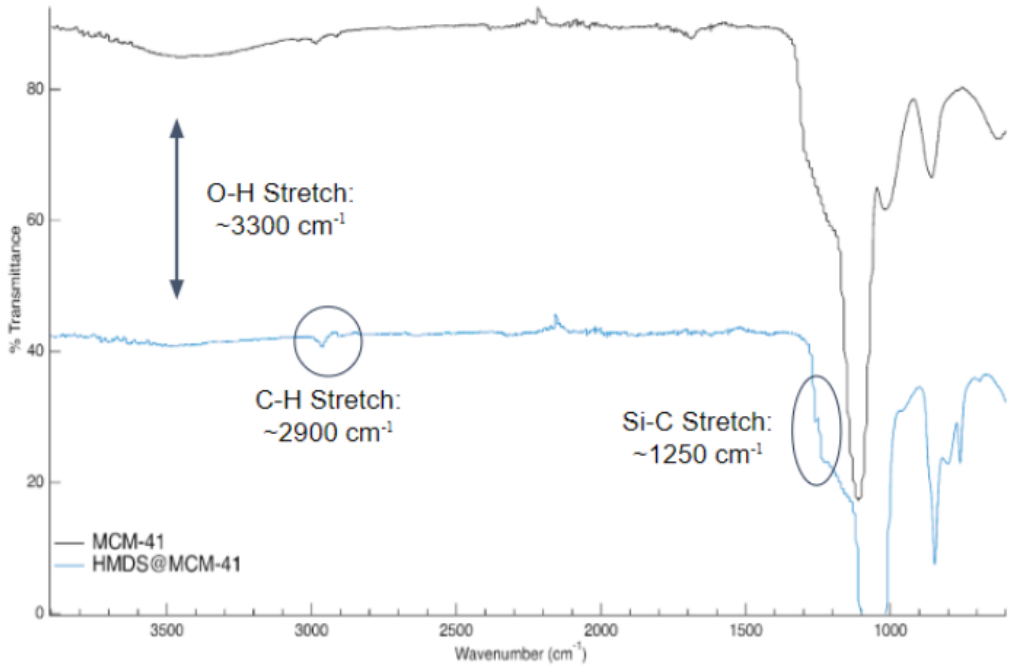

Figure 3.9 IR data of MCM-41 and HMDS@MCM-41 (offset). Note the disappearance of the OH stretch and emergence of C-H and Si-C peaks.

Nitrogen physisorption was also conducted to confirm that porosity was not lost during the functionalization procedure. The HMDS@MCM-41 isotherm was still a type IV isotherm, with a slight reduction in surface area. The hysteresis loop shifted slightly towards lower pressures, closer to the microporous regime. This is indicative of a decrease in pore diameter resulting from the trimethylsilane groups extending from the pore walls, reducing the diameter of pore openings. This is corroborated by the BJH pore distribution, which shows a slight decrease in pore volume and average pore diameter compared to the parent MCM-41 material. The augmented material still displayed high surface area (904 m^2/g) suitable for drug storage and delivery.

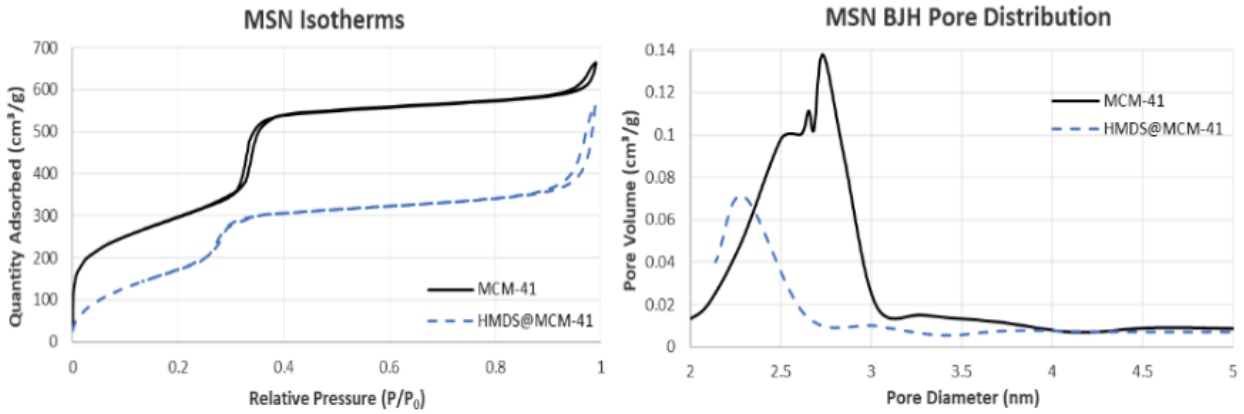

Figure 3.10 Isotherms for the HMDS functionalized and parent MCM-41; reduced pore size indicative of trimethylsilane introduction.

Qualitatively, the HMDS@MCM-41 material was no longer soluble in PBS or other polar solvents, showcasing the hydrophobic nature of the tailored material (imaged in *Appendix Fig. A.4*). Overall, the incorporation of trimethylsilane groups onto the MCM-41 surface was confirmed. To determine if the new surface chemistry would improve amylose interactions, the coating procedure was conducted without undergoing fluorescein loading for HMDS@MCM-41. The resulting sample was named Amylose@HMDS and the procedure outlined in *Appendix A.1.* Nitrogen physisorption was again performed to quantify pore coverage. Compared to HMDS@MCM-41, a substantial decrease in porosity and surface

area occurred. The amylose coated MSN had a reduced surface area of 97 m^2/g, compared to the parent HMDS@MCM-41's surface area of 904 m^2/g. Similar to Coat-1 and Coat-2, however, the 'coated' isotherm retained its type IV shape and mesoporosity. The BJH pore distribution showed a reduced pore volume, but residual presence of mesopores. This data could be explained by partial/inconsistent pore blockage, or by the same independent amylose aggregate formation discovered for the non functionalized MCM-41.

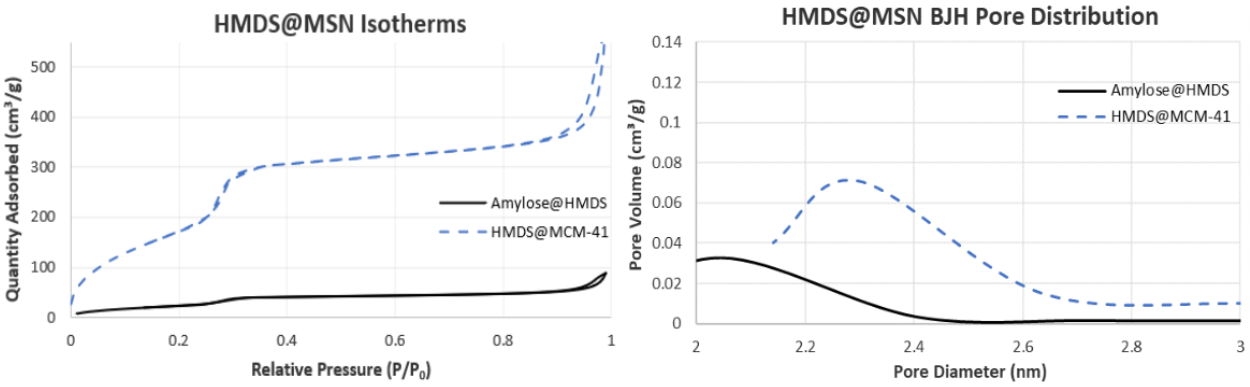

Figure 3.11 HMDS functionalized MCM-41 isotherms before and after the amylose coating. Surface area decreases, yet type IV isotherm shape and mesoporosity are preserved.

TGA was also conducted on HMDS@MCM-41 and Amylose@HMDS to quantify the presence of amylose. HMDS@MCM-41 had only 11.4% weight loss up beyond 100° C, with noticeably less mass loss occurring before 200° C, compared to the parent MCM-41. This implies less water was adsorbed to the surface of the material, which corroborates the surface functionalization reducing hydrophilic interactions. The amylose coated HMDS@MCM-41, however, had 80.6% mass loss by 800° C. The degradation pattern was again consistent for amylose. This suggests that the majority of the sample was amylose. The measured surface area and mesoporosity corresponds to uncoated HMDS@MCM-41 mixed with nonporous amylose. Despite the more nonpolar surface, amylose pore coverage was still not observed.

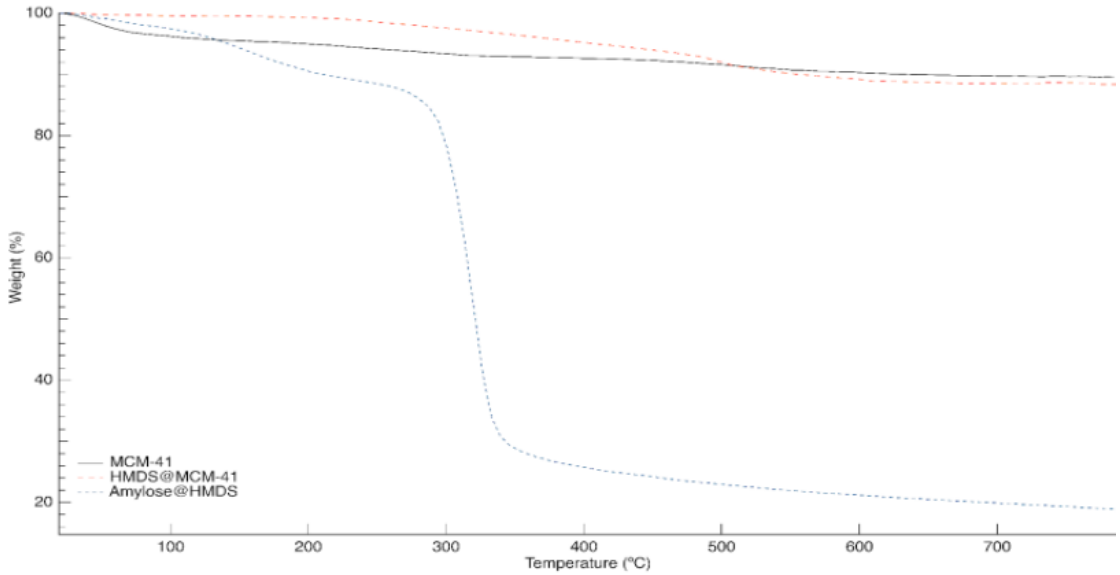

Figure 3.12 TGA data comparing parent MCM-41 with HMDS@MCM-41 before and after starch coat. HMDS@MCM-41 showed less adhered moisture, while the 'coated' sample was primarily amylose

CHAPTER 4

CONCLUSIONS AND PROPOSED WORKS

4.1 Conclusions

Controlled uptake and sustained release of fluorescein were observed in an MCM-41 drug delivery system. Concentration gradient and pH dependent electrostatic interactions between the cargo and MCM-41 surface were determined to be the driving forces of pore loading and unloading. Fluorescein loading efficiency of 95% (corresponding to 0.6% by weight) was consistently reached under acidic solvent impregnation. Higher weight percent loading can be achieved by using higher volumes or concentrations of fluorescein loading solution, allowing tunability of release kinetics and loading amount. Amylose and amylopectin displayed poor surface interactions with bare MCM-41– amylose conglomerates formed independent from the MCM-41, yielding insufficient pore coverage. Surface functionalization with trimethylsilanes improved nonpolar interactions, yet nitrogen physisorption and TGA data suggested mesoporosity and unblocked pores remained after attempted amylose coating of HMDS modified MCM-41. Noncovalent amylose coating and enzyme promoted fluorescein release still proved elusive.

4.2 Suitable Next Steps

The work herein provides proof-of-concept steps towards biopolymer coated MSN for drug delivery. Noncovalent association of the biopolymer shell around the MCM-41 did not improve after HMDS functionalization; more data is required to determine if amylose pore coverage can be obtained by this method. If successful, the different chemical properties of HMDS@MCM-41 will also necessitate a revised loading procedure, with a different solvent. Removing the acidic nature of the MCM-41 may improve fluorescein loading and provides an avenue towards favorable drug loading with nonpolar drugs.

Finally, in the event HMDS@MCM-41 amylose coating is unobtainable, another biopolymer may be considered for pore coverage. The cationic biopolymer chitosan is promising for pH selective drug delivery. The pKa of chitosan is around 6.5 and thus is positively charged at lower pHs.[62] At a pH between the isoelectric point of MCM-41 and the pKa of chitosan, MCM-41 will be deprotonated and negatively charged, promoting more favorable surface interactions with chitosan. Noncovalent endcapping with chitosan might be more attainable than with amylose. To achieve enzyme specific responsiveness, the chitosan coating should be chemically crosslinked to form a robust chitosan cage around the MCM-41, which can avoid pH dependent dissociation. This can be accomplished by targeting the primary amines of chitosan with a carbonyl group and forming a Schiff base. Glutaraldehyde could be used to form Schiff-base linkages connecting chitosan subunits, providing pH independent rigidity. Enzymatic response could be achieved as human lysozyme and bacterial colon enzymes are able to hydrolyze chitosan subunits, which could dissociate the chitosan cage and unblock the pores. This provides a potential avenue towards site specific colonic drug delivery, with applications in colonic chemotherapy.

REFERENCES

1. Price, G.; Deven, A. Drug Bioavailability. *StatPearls*. **2021**. Treasure Island (FL): StatPearls Publishing; 2022 Jan-. Available from: https://www.ncbi.nlm.nih.gov/books/NBK557852/.

2. Karimi, M.; Mirshekari, H.; Aliakbari, M.; et al. Smart Mesoporous Silica Nanoparticles for Controlled-Release Drug Delivery. *Nanotechnol. Rev.* **2016**, *5* (2), 195-207. DOI: 10.1515/ntrev-2015-0057.

3. Manzano, M.; Vallet-Regí, M. Mesoporous Silica Nanoparticles for Drug Delivery. *Adv. Funct. Mater.* **2020**, *30* (2). DOI:10.1002/adfm.201902634.

4. Kuang, Y.; Zhai, J.; Xiao, Q.; et al. Polysaccharide/Mesoporous Silica Nanoparticle-Based Drug Delivery Systems: A Review. *Int. J. Biol. Macromol.* **2021**, *193*, 457-473. DOI: 10.1016/j.ijbiomac.2021.10.142.

5. Gonzalez, G.; Sagarzazu, A.; Zoltan, T. Influence of Microstructure in Drug Release Behavior of Silica Nanocapsules. *J. Drug Deliv.* **2013**. DOI:10.1155/2013/803585.

6. Jadhav, K.; Dumbare, P.; Pande, V. Mesoporous Silica Nanoparticles (MSN): a Nanonetwork and Hierarchical Structure in Drug Delivery. *J. Nanomed. Res.* **2015**, *2* (5), 156-161. DOI: 10.15406/jnmr.2015.02.00043.

7. Slowing, I.; Trewyn, B.; Giri, S.; et al. Mesoporous Silica Nanoparticles for Drug Delivery and Biosensing Applications. *Adv. Funct. Mater.* **2007**, *17* (8), 1225-1236. DOI: 10.1002/adfm.200601191.

8. Doadrio, A.; Salinas, A.; Sánchez-Montero, J.; Vallet-Regí, M. Drug Release From Ordered Mesoporous Silicas. *Curr. Pharm. Des.* **2015**, *21* (42), 6213-819. DOI: 10.2174/138161282 2666151106121419.

9. Popova, T.; Tzankov, B.; Voycheva, C.; et al. Mesoporous Silica MCM-41 and HMS as Advanced Drug Delivery Carriers for Bicalutamide. *J. Drug Deliv. Sci. Technol.* **2021**, *62*, 102340. DOI: 10.1016/j.jddst.2021.102340.

10. Martinez-Carmona, M.; Gun'ko, Y.; Vallet-Regí, M. Mesoporous Silica Materials as Drug Delivery: "The Nightmare" of Bacterial Infection. *Pharmaceuitcs.* **2018**, *10* (4), 279. DOI: 10.3390/pharmaceutics10040279.

11. Argyo, C.; Weiss, V.; Bräuchle, C.; et al. Multifunctional Mesoporous Silica Nanoparticles as a Universal Platform for Drug Delivery. *Chem. Mater.* **2014**, *26*, 435-451. DOI: 10.1021/cm402592t.

12. Giri, S.; Trewyn, B.; Stellmaker, M.; et al. Stimuli-Responsive Controlled-Release Delivery System Based on Mesoporous Silica Nanorods Capped with Magnetic Nanoparticles. *Angew. Chem. Int.* **2005**, *117* (32), 5166-5172. DOI: 10.1002/ange.200501819.

13. Bernardos, A.; Mondragón, L.; Aznar, E.; et al. Enzyme-Responsive Intracellular Controlled Release Using Nanometric Silica Mesoporous Supports Capped with "Saccharides". *ACS Nano.* **2010**, *4* (11), 6353–6368. DOI: 10.1021/nn101499d.

14. Chang, Y.; Yang, J.; Ren, L.; et al. Characterization of Amylose Nanoparticles Prepared via Nanoprecipitation: Influence of Chain Length Distribution. *Carbohydr. Polym.* **2018**, *194*, 154–160. DOI: 10.1016/j.carbpol.2018.03.104.

15. Subramanian, K.; Vediappan, V. Hydrogels: Classification, Synthesis, Characterization, and Applications. *Encyclopedia of Biomedical Polymers and Polymeric Biomaterials.* **2015**, 3879-3892. DOI: 10.1081/E-EBPP-120049894.

16. Dong, Y.; Chang, Y.; Wang. Q.; et al. Effects of Surfactants on Size and Structure of Amylose Nanoparticles Prepared by Precipitation. *Bull. Mater. Sci.* **2016**, *39*, 35–39. DOI: 10.1007/s12034-015-1115-5.

17. Genomid. *Introduction to Pharmacokinetics: Four Steps in a Drug's Journey Through the Body.* https://genomind.com/providers/introduction-to-pharmacokinetics-four-steps-in-a-drugs-journey-through-the-body/ (accessed 2022-07-19).

18. Vertzoni, M.; Augustijns, P.; Grimm, M.; et al. Impact of Regional Differences Along the Gastrointestinal Tract of Healthy Adults on Oral Drug Absorption: An UNGAP Review. *Eur. J. Pharm. Sci.* **2019**, *134*, 153-175. DOI:10.1016/j.ejps.2019.04.013.

19. Fender, A.; Dobrev, D. Bound to Bleed: How Altered Albumin Binding May Dictate Warfarin Treatment Outcome. *Int. J. Cardiol. Heart. Vasc.* **2019**, *22*, 214-215. DOI: 10.1016/j.ijcha.2019.02.007.

20. Grasela, T.; Lukacova, V.; Morris, D.; et al. Human PK Prediction and Modeling. *Med. Chem.* **2017**, *49* (2), 169–178. DOI: 10.1124/dmd.120.000202.

21. Herman, T.; Santos, C. First Pass Effect. *StatPearls.* **2022**. Treasure Island (FL): StatPearls Publishing; 2022 Jan-. Available from: https://www.ncbi.nlm.nih.gov/books/NBK551679/.

22. Kato, Motohiro. Intestinal First-Pass Metabolism of CYP3A4. *Eur. J. Drug Metab. Pharmacokinet.* **2008**, *23*, 87–94. DOI: 10.2133/dmpk.23.87.

23. McDonnell, A.; Dang, C. Basic Review of the Cytochrome P450 System. *J. Adv. Pract. Oncol.* **2013**, *4* (4), 263-8. DOI: 10.6004/jadpro.2013.4.4.7.

24. Tam, Y. Individual Variation in First-Pass Metabolism. *Clin. Pharmacokinet.* **1993**, *25* (4), 300-328. DOI: 10.2165/00003088-199325040-00005.

25. Wongrakpanich, S.; Wongrakpanich, A.; Melhado, K.; et al. A Comprehensive Review of Non-Steroidal Anti-Inflammatory Drug Use in The Elderly. *Aging Dis.* **2018**, *9* (1), 143-150. DOI: 10.14336/AD.2017.0306.

26. American Cancer Society. *How Chemotherapy Drugs Work.* https://www.cancer.org/treatment/treatments-and-side-effects/treatment-types/chemotherapy/how-chemotherapy-drugs -work.html (accessed 2022-07-26).

27. BioNumbers. *How Quickly Do Different Cells in the Body Replace Themselves?* http://book.bionumbers.org/how-quickly-do-different-cells-in-the-body-replace-themselves/ (accessed 2021-04-26).

28. Bio. *New Study Shows the Rate of Drug Approvals Lower than Previously Reported.* https://archive.bio.org/media/press-release/new-study-shows-rate-drug-approvals-lower-previously-reported (accessed 2021-04-13).

29. CU Boulder Today. *Gender-Bending Fish Problem in Colorado Creek Mitigated by Treatment Plant Upgrade.* https://www.colorado.edu/today/2010/06/21/gender-bending-fish-problem-colorado-creek-mitigated-treatment-plant-upgrade (accessed 2022-07-01).

30. Vajda, A.; Barber, L.; Gray, J.; et al. Demasculinization of Male Fish by Wastewater Treatment Plant Effluent. *Aqua. Tox.* **2011**, *103* (3-4), 213-221. DOI: 10.1016/J.AQUATOX.2011.02.007.

31. Vajda, A.; Barber, L.; Gray, J.; et al. Reproductive Disruption in Fish Downstream from an Estrogenic Wastewater Effluent. *Environ. Sci. Technol.* **2008**, *42* (9), 3407–3414. DOI: 10.1021/es0720661.

32. Blazer, V.; Walsh, H.; Shaw, C.; et al. Indicators of Exposure to Estrogenic Compounds at Great Lakes Areas of Concern: Species and Site Comparisons. *Environ. Monit. Assess.* **2018**, *190* (10), 577. DOI: 10.1007/s10661-018-6943-5.

33. Congressional Research Service [R44832]. *Frequently Asked Questions About Prescription Drug Pricing and Policy. Rev. 05.2021.* https://crsreports.congress.gov/product/pdf/R/R44832.

34. Nurses. *Organization for Economic Co-operation and Development.* https://data.oecd.org/healthres/nurses.htmindicator-chart (accessed 2022-07-24).

35. Vallet-Regi, M.; Rámila, A.; Del Real, R.; Pérez-Pariente, J. A New Property of MCM-41: Drug Delivery System. *Chem. Mater.* **2001**, *13*, 308. DOI: 10.1021/cm0011559.

36. Mamaeva, V.; Sahlgren, C.; Lindén, M. Mesoporous Silica Nanoparticles in Medicine–Recent Advances. *Adv. Drug Deliv.* **2013**, *65* (5), 689-702. DOI: 10.1016/j.addr.2012.07.018.

37. Croissant, J.; Fatieiev, Y.; Almalik, A.; Khashab, N. Mesoporous Silica and Organosilica Nanoparticles: Physical Chemistry, Biosafety, Delivery Strategies, and Biomedical Applications. *Adv. Healthc. Mater.* **2017**, *7* (4). DOI: 10.1002/adhm.201700831.

38. Zhang, Y.; Poon, W.; Tavares, A.; et al. Nanoparticle-liver Interactions: Cellular Uptake and Hepatobiliary Elimination. *J. Control. Release.* **2016**, *240*, 332-348. DOI: 10.1016/j.jconrel.2016.01.020.

39. Feng, C.; Tapas, R.; Nayak, S.; et al. In Vivo Tumor Vasculature Targeted PET/NIRF Imaging with TRC105(Fab)-Conjugated, Dual-Labeled Mesoporous Silica Nanoparticles. *Mol. Pharm.* **2014**, *11* (11), 4007-4014. DOI: 10.1021/mp500306k.

40. Braun, K.; Pochert, A.; Beck, M.; et al. Dissolution Kinetics of Mesoporous Silica Nanoparticles in Different Simulated Body Fluids. *J. Solgel. Sci. Technol.* **2016**, 79. DOI: 10.1007/s10971-016-4053-9.

41. Lickiss, P. The Synthesis and Structure of Organosilanols. *Adv. Inorg. Chem.* **1995**, *42*, 147– 262. DOI:10.1016/S0898-8838(08)60053-7.

42. Liu, H.; Xu, P. Smart Mesoporous Silica Nanoparticles for Protein Delivery. *Nanomaterials.* **2019**, *9* (4). DOI: 10.3390/nano9040511.

43. Du, P.; Nguyen, T.; Thuy, C.; et al. Aminopropyl Functionalized MCM-41: Synthesis and Application for Adsorption of Pb(II) and Cd(II). *Adv. Mater. Sci. Eng.* **2019**. DOI: 10.1155/2019/8573451.

44. Shariatinia, Z.; Pourzadi, N.; Darvishi, S. Tert-Butylamine Functionalized MCM-41 Mesoporous Nanoparticles as Drug Carriers for the Controlled Release of Cyclophosphamide Anticancer Drug. *Surf. Interfaces.* **2021**, *22*, 100842. DOI: 10.1016/J.SURFIN.2020.100842.

45. Bao, G.; Mitragotri, S.; Tong, S. Multifunctional Nanoparticles for Drug Delivery and Molecular Imaging. *Annu. Rev. Biomed. Eng.* **2013**, *15*, 253-82. DOI: 10.1146/annurev-bioeng-071812-152409.

46. Charles, T.; Kresge, J.; Vartuli, W.; et al. The Discovery of ExxonMobil's M41S Family of Mesoporous Molecular Sieves. *Stud. Surf. Sci. Catal.* **2004**, *148*, 53-72. DOI: 10.1016/S0167-2991(04)80193-9.

47. Dayane, O.; Andrada, A. Synthesis of Ordered Mesoporous Silica MCM-41 With Controlled Morphology for Potential Application in Controlled Drug Delivery Systems. *Ceramica.* **2019**, *65*, 170-179. DOI: 10.1590/0366-69132019653742509.

48. Sang, W.; Ching, O. Tailoring MCM-41 Mesoporous Silica Particles Through Modified Sol-Gel Process for Gas Separation. *AIP Conference Proceedings.* **2017**, *1891*, 020147. DOI: 10.1063/1.5005480.

49. Hoffmann, F.; Cornelius, M.; Morell, J. Silica-Based Mesoporous Organic–Inorganic Hybrid Materials. *Angew. Chem. Int. Ed.* **2006**, *45* (20), 3216-51. DOI: 10.1002/anie.200503075.

50. Johansson, E.; Cordoba, J.; Oden, M. The Effects on Pore Size and Particle Morphology of Heptane Additions to the Synthesis of Mesoporous Silica SBA-15. *Micropor. Mesopor. Mat.* **2010**, *133*, 66–74. DOI: 10.1016/j.micromeso.2010.04.016.

51. Deodhar, G.; Adams, M.; Trewyn, B. Controlled Release and Intracellular Protein Delivery From Mesoporous Silica Nanoparticles. *Biotechnol. J.* **2017**, *12* (1). DOI: 10.1002/biot.201600408.

52. Martínez-Edo, G.; Balmori, A.; Pontón, I.; et al. Functionalized Ordered Mesoporous Silicas (MCM-41): Synthesis and Applications in Catalysis. *Catalysts.* **2018**, *8* (12), 617. DOI: 10.3390/catal8120617.

53. Coster, D.; Blumenfeld, A.; Fripiat, J. Lewis Acid Sites and Surface Aluminum in Aluminas and Zeolites: A High-Resolution NMR Study. *J. Phys. Chem.* **1994**, *98* (24), 6201-6211. DOI: 10.1021/j100075a024.

54. Vasconcelos, T.; Sarmento, B.; Costa, P. Solid Dispersions as Strategy to Improve Oral Bioavailability of Poor Water Soluble Drugs. *Drug. Discov. Today.* **2007**, *12* (23), 1068-75. DOI:10.1016/j.drudis.2007.09.005.

55. Nakamura, Y.; Mochida, A.; Choyke, P.; et al. Nanodrug Delivery: Is the Enhanced Permeability and Retention Effect Sufficient for Curing Cancer? *Bioconjug. Chem.* **2016**, *27* (10), 2225-2238. DOI: 10.1021/acs.bioconjchem.6b00437.

56. Kalyane, D.; Raval, N.; Maheshwari, R.; et al. Employment of Enhanced Permeability and Retention Effect (EPR): Nanoparticle-Based Precision Tools for Targeting of Therapeutic and Diagnostic Agent in Cancer. *Mater. Sci. Eng.* **2019**, *98*, 1252-1276. DOI: 10.1016/j.msec.2019.01.066.

57. Acharya, S.; Sahoo, S. PLGA Nanoparticles Containing Various Anticancer Agents and Tumour Delivery by EPR Effect. *Adv. Drug. Deliv.* **2011**, *63*, 170-183. DOI:10.1016/j.addr.2010.10.008.

58. Rehman, A.; Jafari, S.; Tong, Q.; et al. Drug Nanodelivery Systems Based on Natural Polysaccharides Against Different Diseases. *Adv. Colloid. Interfac. Sci.* **2020**, 284. DOI: 10.1016/j.cis.2020.102251.

59. Hariyadi, D.; Islam, N. Current Status of Alginate in Drug Delivery. *Adv. Pharmacol. Pharm. Sci.* **2020**, 8886095. DOI: 10.1155/2020/8886095.

60. Hu, L.; Sun, C.; Song, A.; et al. Alginate Encapsulated Mesoporous Silica Nanospheres as a Sustained Drug Delivery System for the Poorly Water-Soluble Drug Indomethacin. *Asian J. Pharm. Sci.* **2014**, *9* (4), 183-190. DOI: 10.1016/j.ajps.2014.05.004.

61. Li, X.; Wang, Z.; Xia, H. Ultrasound Reversible Response Nanocarrier Based on Sodium Alginate Modified Mesoporous Silica Nanoparticles. *Front. Chem.* **2019**, *11* (7), 59. DOI: 10.3389/fchem.2019.00059.

62. Muxika, A.; Etxabide, A.; Uranga, J.; et al. Chitosan as a Bioactive Polymer: Processing, Properties and Applications. *Int. J. Biol. Macromol.* **2017**, *105* (2), 1358-1368. DOI: 10.1016/j.ijbiomac.2017.07.087.

63. Hu, X.; Wang, Y.; Peng, B. Chitosan-Capped Mesoporous Silica Nanoparticles as pH-Responsive Nanocarriers for Controlled Drug Release. *Chem. Asian. J.* **2014**, *9*, 319-327. DOI 10.1002/asia.201301105.

64. Navid, N.; Hassan, K.; Mojtaba, B.; et al. Delivery of Curcumin by a pH-Responsive Chitosan Mesoporous Silica Nanoparticles for Cancer treatment. *Artif. Cells. Nanomed. Biotech.* **2018**, *46*, 75-81, DOI: 10.1080/21691401.2017.1290648.

65. Andrés, F.; Doblado-Maldonado, S.; Gomand, Bart. Methodologies for Producing Amylose: A Review. *Crit. Rev. Food. Sci. Nutr.* **2017**, *57* (2), 407-417. DOI: 10.1080/10408398.2014.954030.

66. Faisal, M.; Kou, T.; Zhong, Y.; et al. High Amylose-Based Bio Composites: Structures, Functions and Applications. *Polymers (Basel).* **2022**, *14* (6), 1235. DOI: 10.3390/polym14061235.

67. Williams, P. Determination of α- and β-Amylase. In *Encyclopedia of Analytical Science*, 2nd Ed.; Elsevier Ltd, 2005; pp 544-546.

68. Sundarram, A.; Murthy, T. α-Amylase Production and Applications: A Review. *Appl. Environ. Microbiol.* **2014**, *2* (4), 166-175. DOI: 10.12691/jaem-2-4-10.

69. Clinical Advisor. *Oral Medication Management in Patients With Dysphagia*. https://www.clinicaladvisor.com/counselingconnection/oral-medication-management-in-patients-with-dysphagia/ (accessed 2022-09-29).

70. Matull, W.; Pereira, S.; O'Donohue, J. Biochemical Markers of Acute Pancreatitis. *J. Clin. Pathol*. **2006**, *59* (4), 340-344. DOI: 10.1136/jcp.2002.002923.

71. Othman, Z. A Review: Fundamental Aspects of Silicate Mesoporous Materials. *Materials (Basel)*. **2012**, *5* (12), 2874–902. DOI: 10.3390/ma5122874.

72. Goworek, J.; Kierys, A.; Gac, W.; et al. Thermal Degradation of CTAB in as-Synthesized MCM-41. *J. Therm. Anal. Calorim*. **2009**, *96*, 375–382. DOI: 10.1007/s10973-008-9055-6.

73. Sulpizi, M.; Gaigeot, P.; Sprik, M. The Silica-Water Interface: How the Silanols Determine the Surface Acidity and Modulate the Water Properties. *J. Chem. Theory. Comput*. **2012**, *8*, 1037-47. DOI: 10.1021/ct2007154.

74. Nassima, B.; Benhamou, A.; Abdelkader, D. Synthesis and Modification of a Mesoporous Material Type MCM-41 by an Amine for the Adsorption of Organic Pollutants: Anionic and Cationic Dyes. *BioRxiv*. [Preprint.] **2017**. DOI:10.1101/118182.

75. Lavis, L.; Rutkoski, T.; Raines, R. Tuning the pK(a) of Fluorescein to Optimize Binding Assays. *Anal. Chem*. **2007**, *79*, 6775-82. DOI:10.1021/ac070907g.

76. McGrance, S.; Cornell, H.; Rix, C. A Simple and Rapid Colorimetric Method for the Determination of Amylose in Starch Products. *Starch*. **1998**, *50* (4), 158-163. DOI: 10.1002/(SICI)1521-379X(199804)50:4¡158::AID-STAR158¿3.0.CO;2-7.

77. Xingxun L.; Long, Yu.; Hongsheng, L.; et al. Thermal Decomposition of Corn Starch with Different Amylose/Amylopectin Ratios in Open and Sealed Systems. *Cereal Chem*. **2009**, *86* (4), 383-385. DOI: 10.1094/CCHEM-86-4-0383.

78. Kandel, K.; Althaus, S.; Peeraphatdit, C.; et al. Solvent-Induced Reversal of Activities between Two Closely Related Heterogeneous Catalysts in the Aldol Reaction. *ACS Catalysis*. **2013**, *3* (2), 265-271. DOI: 10.1021/cs300748g.

79. Anwander, R.; Nagl, I.; Widenmeyer, M.; et al. Surface Characterization and Functionalization of MCM-41 Silicas via Silazane Silylation. *J. Phys. Chem. B*. **2000**, *104* (15), 3532-3544. DOI: 10.1021/jp993108d.

80. Lorenti, J.; Scolari, E.; Cabral, N.; et al. Isomerization and Epimerization of Glucose Catalyzed by Sn-Containing Mesoporous Silica. *Ind. Eng. Chem. Res*. **2021**, *60* (35), 12821-12833. DOI: 10.1021/acs.iecr.1c0178.

81. WebSpectra. *Problems in NMR and IR Spectroscopy*. https://webspectrachem.ucla.edu//index.html (accessed 2022-09-30).

82. Gelest. *Infrared Analysis of Organosilicon Compounds: Spectra- Structure Correlations*. https://www.gelest.com/wp-content/uploads/ 5000A-Section1-Infrared Analysis.pdf (accessed 2022-10-2).

APPENDIX

SUPPLEMENTAL INFORMATION

A.1 Alternate Methods

Coat-1 and Coat-2 were prepared according to the same general methodology as in *2.5 Starch Coating*, but with variations to achieve different quantities of amylose precipitation. Coat-1 was prepared by dissolving 50 mg of loaded MCM-41 in a minimal amount of fluorescein in PBS solution, which was then added dropwise into 5 mL of a 1% amylose DMSO:water solution. Coat-2 was prepared to precipitate amylose in excess, by combining 8 mL of the same amylose solution with loaded MCM-41, sonicating, and adding 25 mL of methanol to rapidly precipitate amylose from solution.

Other samples were prepared with similar variations, including different amylose solution concentrations and volumes, use of amylopectin instead of amylose, different solvent choices, altering the order of addition, etc. Overall, products from alternative coating methodologies were qualitatively the same and did not show enzymatic response, and as such, were not characterized to the same length as Coat-1 and Coat-2.

Amylose@HMDS was prepared by combining 25 mg of HMDS@MCM-41 with 5 mL of a 1% amylose in 90:10 DMSO:water solution. The reaction mixture was sonicated for 5 minutes to dissolve the MSN, after which, 15 mL of methanol was added to rapidly precipitate out the amylose. The mixture was centrifuged, decanted, rinsed with methanol to remove excess amylose and residual DMSO, and freeze dried.

A.2 Additional Data

A.2.1 Electron Microscopy

SEM was used to view the particle morphology and determine average particle size. From this, it was confirmed that both silica syntheses yielded succinct nanoparticles of consistent size, rather than a bulk or unordered material. Initially, clarity and resolution of

the SEM images were poor– a result of static charging on the silica material. SEM images have highest clarity when the analyte is conductive. Silica is a poorly conductive covalent framework, which leads to static build up obscuring the image quality. To address this, the samples underwent a gold sputtering to improve conductivity and clarity. These improved images are presented in *Fig. 3.1* in section *3.1.* The SEM images prior to gold coating are shown in *Fig. A.1.* Quantitative observations are limited with these images. They do suggest that succinct particle formation has occurred, and that the MCM-41 was smaller than the Stöber silica.

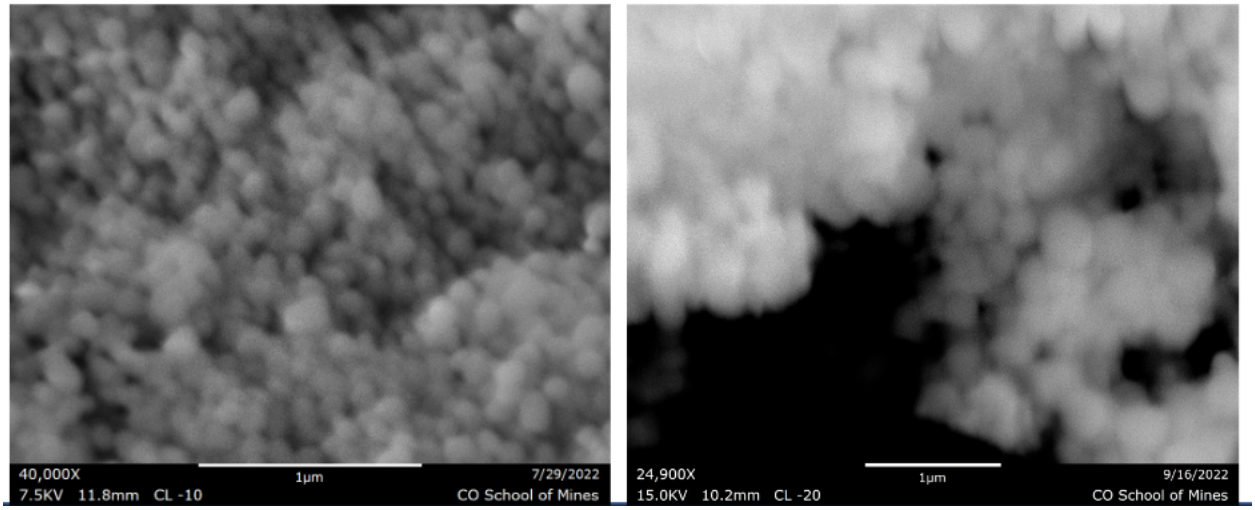

Figure A.1 SEM image of MCM-41 (left) and Stöber silica (right), showing nanoparticle formation. Poor image quality due to static buildup on the nonconductive silica.

A.2.2 Nitrogen Physisorption

Nitorgen physisorption on the synthesized Stöber silica generated a type III isotherm, indicative of a nonporous material with pore gas/surface interactions. No hysteresis was observed in the mesoporous range. A gap between adsorption and desorption branches is observed at relative pressures above 0.9. This corresponds to textural porosity, which arises as gaps inbetween separate spherical nanoparticles fill and empty of gas at high relative pressures. This porosity does not correspond to heightened surface area, but is an artifact

of surface analysis of nanoparticles. Further, it corroborates the formation of separate spherical nanoparticles.

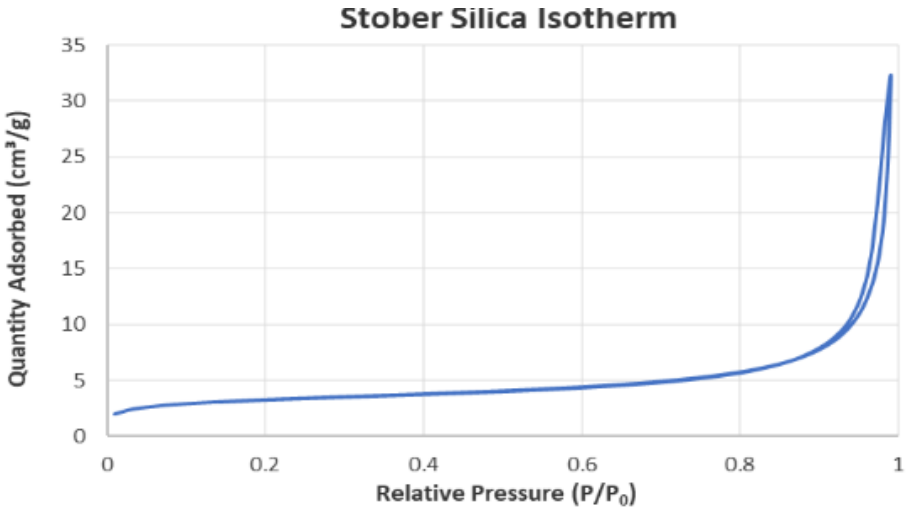

Figure A.2 Nitrogen physisorption isotherm for Stöber silica. Nonporous type III shape.

The BET calculated surface areas of the bare MCM-41 materials characterized in *Results and Discussions* are tabulated below in *Table A.1.* Broadly, it can be seen that MCM-41 had expected high surface area, Stöber silica was nonporous, and the surface area of the loaded trials decreased following fluorescein impregnation. The coated trials displayed reduce surface area, but retained mesoporosity consistent with separate amylose aggregation. Further analysis is needed to reveal a trend in pore volume corresponding to fluorescein loading, as loading did not significantly decrease reported pore volume. BJH pore distribution did however suggest a reduction in average pore diameter following cargo loading.

Table A.1 Tabulated surface area data for unfunctionalized materials.

Sample	MCM-41	Stöber	Load-1	Load-2	Coat-1	Coat-2
Surface Area (m^2/g)	1,070	11	930	860	440	260
Pore Volume (cm^3/g)	1.002	N/A	1.072	0.992	0.336	0.286

The BET calculated surface areas of the HMDS augmented MCM-41 materials are tabulated below in *Table A.2*. The incorporation of trimethylsilane moieties slightly lowered surface area and pore volume. The decrease in the coated sample's surface area was indicative of physical mixing and not pore coverage.

Table A.2 Tabulated surface area data for trimethylsilane materials.

Sample	MCM-41	HMDS@MCM-41	Amylose@HMDS
Surface Area (m^2/g)	1,070	904	97
Pore Volume (cm^3/g)	1.002	0.781	0.115

A.2.3 Thermal Gravimetric Analysis

Weight loss percents from all conducted TGA trials are compiled below. The weight loss percentages were found by comparing the sample weight at 100° C to the weight at 800° C. This excluded weight loss occurring from surface adhered moisture or residual solvent. The degredation patterns of substational weight loss were consistent with amylose and suggested reduced surface area corresponded to increased amounts of amylose in the mixture.

Table A.3 Tabulated TGA weight loss data beyond 100° C.

Sample	MCM-41	Stöber	Coat-1	Coat-2	HMDS@MCM-41	Amylose@HMDS
Weight Loss	6.9 %	8.2%	27.5%	63.0%	11.2%	80.6%

A.2.4 Qualitative Observations

The colorimetric properties of fluorescein provided simple and direct qualitative observations visually. After the loading procedure, MCM-41 alone released fluorescein out into solution, shown in *Fig. A.3* It was also visualized during the loading procedure that the MCM-41 loaded samples would clarify their loading solutions overtime, as fluorescein excited solution to fill the pores, while the Stöber silica did not visually change the solution.

A triiodine solution was used to visually test the presence of amylose before and after enzyme treatment. The reagent changed color in the presense of amylose in the control trial and remained yellow in the trial with amylase solution present, signifying the functionality of the enzyme. While amylase is a physiological enzyme that functions best at 37° C, the enzyme proved effective at complete hydrolysis of the amylose samples over the course of an hour, so room temperature experimentation was deemed sufficient for rapid qualitative analysis of coating procedures.

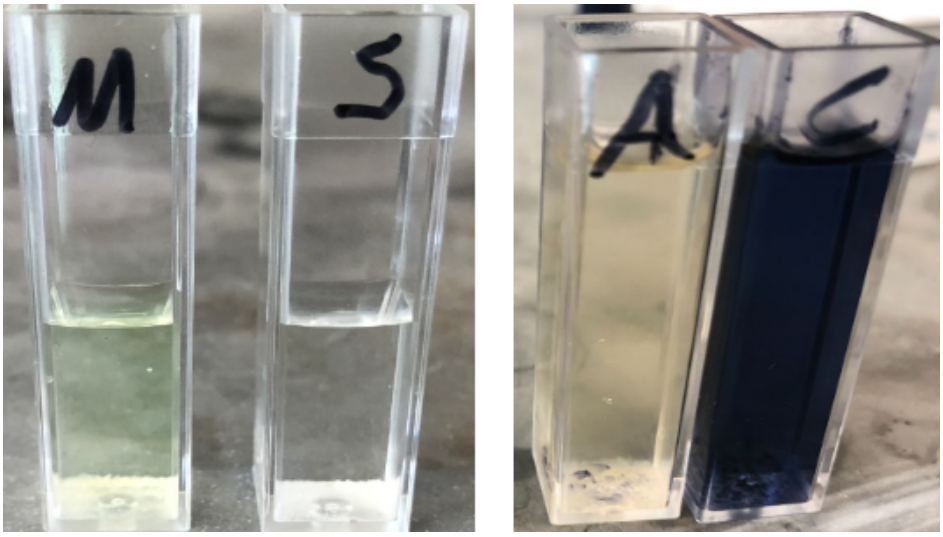

Figure A.3 Colorimetric data. Left: visual release of fluorescein from MCM-41 and not from Stöber silica. Right: enzyme activity shown for Coat-1 release, amylose present only in amylase-free control.

After trimethylsilane functionalization of MCM-41, the emergent nonpolar properties of HMDS@MCM-41 were observed. The material was insoluble in PBS over the course of several hours and magnetic stirring (image shown in *Fig. A.4*. This qualitatively confirmed the surface augmentation of the material.

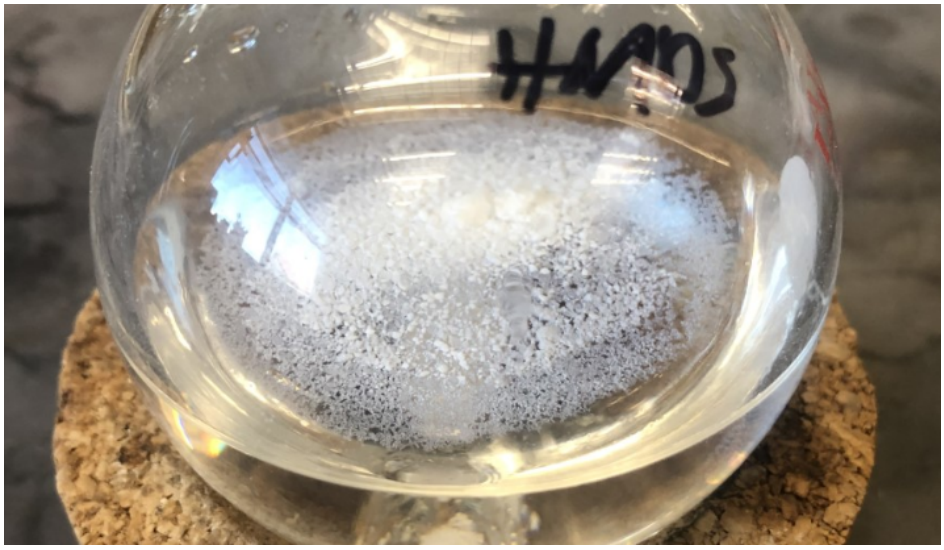

Figure A.4 Image of HMDS@MCM-41 in fluorescein/PBS loading solution. Functionalized material no longer soluble in polar solvents.